Title

Thermodynamics of Anharmonic Systems: Uncoupled Mode Approximations for Molecules.

Journal

Journal of chemical theory and computation, 12(6)

ISSN

1549-9618

Authors

Li, Yi-Pei
Bell, Alexis T
Head-Gordon, Martin

Publication Date

2016-06-01

DOI

10.1021/acs.jctc.5b01177

Peer reviewed

Thermodynamics of Anharmonic Systems: Uncoupled Mode Approximations for Molecules

*Yi-Pei Li[1], Alexis T. Bell[1,3], and Martin Head-Gordon[*2,3]*

[1]Department of Chemical and Biomolecular Engineering, University of California, Berkeley, California 94720-1462

[2]Department of Chemistry, University of California, Berkeley, California 94720-1462

[3]Chemical Sciences Division, Lawrence Berkeley National Laboratory, Berkeley, California 94720

Submitted to
Journal of Chemical Theory and Computation
December 11, 2015
Revised version submitted March 13, 2016.

***Corresponding author:** Martin Head-Gordon: mhg@cchem.berkeley.edu

Keywords: Entropy, Enthalpy, Heat Capacity, Partition function, Anharmonicity, Rigid rotor, Harmonic oscillator, Internal rotor.

Abstract:

The partition functions, heat capacities, entropies, and enthalpies of selected molecules were calculated using uncoupled mode (UM) approximations, where the full-dimensional potential energy surface for internal motions was modeled as a sum of independent one-dimensional potentials for each mode. The computational cost of such approaches scales the same with molecular size as standard harmonic oscillator vibrational analysis using harmonic frequencies (HO^{hf}). To compute thermodynamic properties, a computational protocol for obtaining the energy levels of each mode was established. The accuracy of the UM approximation depends strongly on how the one-dimensional potentials of each modes are defined. If the potentials are determined by the energy as a function of displacement along each normal mode (UM-N), the accuracies of the calculated thermodynamic properties are not significantly improved versus the HO^{hf} model. Significant improvements can be achieved by constructing potentials for internal rotations and vibrations using the energy surfaces along the torsional coordinates and the remaining vibrational normal modes, respectively (UM-VT). For hydrogen peroxide and its isotopologs at 300 K, UM-VT captures more than 70% of the partition functions on average. By contrast, the HO^{hf} model and UM-N can capture no more than 50%. For a selected test set of C2 to C8 linear and branched alkanes and species with different moieties, the enthalpies calculated using the HO^{hf} model, UM-N, and UM-VT are all quite accurate comparing with reference values though the RMS errors of the HO model and UM-N are slightly higher than UM-VT. However, the accuracies in entropy calculations differ significantly between these three models. For the same test set, the RMS error of the standard entropies calculated by UM-VT is ~~2.~~2.~~52~~18 cal mol^{-1} K^{-1} at 1000 K. By contrast, the RMS error obtained using the HO model and UM-N are ~~8.49~~6.42 and ~~6.89~~5.73 cal mol^{-1} K^{-1}, respectively. For a test set composed of nine alkanes ranging from C5 to C8,

the heat capacities calculated with the UM-VT model agree with the experimental values to within a RMS error of ~~0.73~~0.78 cal mol^{-1} K^{-1}, which is less than one-third of the RMS error of the HO^{hf} (~~3.14~~2.69 cal mol^{-1} K^{-1}) and UM-N (~~2.33~~2.41 cal mol^{-1} K^{-1}) models.

Introduction:

Recent advances in ab initio calculations have opened the door towards quantitative understanding of challenging chemical problems such as zeolitic reactions or solution-phase chemistries.[1–5] With on-going developments, the accuracy of electronic energy calculations via density functional theory has been greatly improved,[6] although not yet to the level of chemical accuracy, which is in thermochemistry understood as a 95% confidence limit of ± 1 kcal/mol.[7] However, to compare with quantities measured directly by experiments, calculations of thermodynamic properties at finite temperatures are often essential. For molecular systems, this involves computing vibrational energy levels, which is in principle a challenging problem because it requires modeling the full-dimensional potential energy surface, which is often computationally prohibitive except for extremely small systems. The problem can be greatly simplified by assuming that vibrational modes behave like harmonic oscillators (HO) so that all the energy levels as well as thermodynamic functions can be derived from fundamental frequencies measured by experiments. The standard computational approach is less accurate because experimental fundamental frequencies are replaced by the harmonic frequencies calculated by normal mode analysis (to maintain this distinction, we shall abbreviate it as HO^{hf}).

Formatted: Font: (Default) Times New Roman, 12 pt, Font color: Black, Pattern: Clear

Accordingly, the harmonic approximation faces many limits especially for low frequency modes whose potential energy surface (PES) deviates significantly from a quadratic potential. For instance, as outlined in detail in previous publications, torsions and intermolecular motions of weakly bound molecular clusters are notoriously difficult to handle because their PESs are highly anharmonic.[8–11] The harmonic approximation fails to describe many features of vibrational spectroscopy even for high frequency modes, such as Fermi resonances, as well as tending to overestimate fundamental frequencies. For this reason, zero point energies (ZPEs) derived from harmonic frequencies are often down-scaled.[12,13] Accurate methods for treating the vibrational energy levels for small systems include those utilizing complete quartic force fields,[14–18] and vibrational self-consistent field theory (VSCF),[19–21] perturbation

theory (VPT),[22–26] configuration interaction (VCI),[27–30] and coupled cluster theory (VCC),[31–33] which correct the harmonic reference for higher than quadratic terms. These methods, particularly the higher accuracy variants, have had significant success for small systems, but, with the possible exception of the lower accuracy VSCF and VPT2, are not generally viable for larger molecules.

Significant efforts have also been made to improve the accuracy of the calculated thermodynamic quantities of anharmonic systems. Path integral Monte Carlo (PIMC) and path integral molecular dynamics (PIMD) provide attractive fully numerical schemes to accurately calculate quantum mechanical partition functions with anharmonicity and mode-mode coupling effects taken into account, providing that the temperature of interest is sufficiently high, so that integration over inherently discrete levels is warranted.[34–36] However, due to high computational costs, applications of path integral methods are usually restricted to small systems. On the other hand, methods that represent the full-dimensional PES with tractable functions are more computationally feasible for medium or large size systems though mode-mode coupling effects must inevitably be neglected, at least to some extent.[37] The simplest model following this philosophy is, of course, the HO^{hf} model, which treats all the modes as independent springs with quadratic potentials. The HO^{hf} model is very attractive computationally because only the second derivatives of energies at the critical point have to be computed. Moreover, analytical solutions for the energy levels of quadratic potentials exist so that partition functions can also be derived analytically. More sophisticated models have been proposed for specific cases where the energy surface deviates from a quadratic potential. For instance, truncated Fourier series and Taylor series have been used to approximate the PESs of torsions and anharmonic vibrations.[9,11,38–40] In these models, coupling between modes is often neglected so that the complexity of the problem does not grow exponentially with the size of the system. The accuracy of this approach is, of course, governed by how well the potential function represents the energy surface. Though simple functions such as cosines and low-order truncated polynomials are often chosen to minimize the effort in solving for the energy

levels,[9,11,38] it is usually challenging for non-experts to assess the errors in computed thermodynamic properties due to discrepancies between the model and the real energy surface.

This motivates us to pursue an improved general representation for the PES of complex molecules which still permits direct calculation of thermodynamic properties. In this work, we present a computational protocol solving for the energy levels of PESs represented by cubic splines. With a proper sampling scheme, cubic spline interpolations can accurately represent the PES of a mode, no matter whether it is a nearly harmonic bond stretch, or a highly anharmonic torsion. Our goal is to approach the limit of accuracy that is possible within the uncoupled mode (UM) approximation, so that all modes are treated independently. Remaining errors are then directly due to mode coupling. In this study, two sampling schemes were examined. One is to sample along the direction of each normal mode (UM-N). This sampling scheme has been adopted previously by Sauer and coworkers to study the effect of anharmonic vibrations on adsorption thermodynamics of small molecules with fourth and sixth order polynomials.[9–11] Hoping to generalize the methodology to larger molecules where internal rotations are important effects, we developed another scheme where sampling of vibrations and internal rotations (UM-VT) were carried out separately, which. ~~This~~ can be done by projecting torsional modes out of the Hessian matrix and then separately modeling the PES along the torsional coordinates of rotors and along the eigenvectors of the projected Hessian. The accuracies of the HO^{hf} model, UM-N, and UM-VT were benchmarked for selected molecules against partition functions calculated by path integral methods, heat capacities measured by experiments, as well as enthalpies and entropies derived from statistical mechanics based on spectral data. We found that UM-VT significantly outperformed UM-N and the HO^{hf} model in partition function, heat capacity, and entropy calculations. In enthalpy calculations, these three models performed almost equally well, but a slightly smaller error was obtained for UM-VT. The advantage of UM-VT is that it allows a treatment of anharmonicity for which computational cost scales the same as the HO^{hf} model since it requires only a number of additional single

point calculations along each independent mode or torsion.

Methods:

The details of how to derive energy levels of a system with cubic spline representations for the 1-dimensional PESs are documented in this section. The starting point for any uncoupled mode (UM) model, as documented in detail in previous studies,[9–11,41] are the eigenvectors of the mass-weighted Hessian (i.e. the normal modes)

$$\hat{H} = M^{-1/2}\ HM^{-1/2} \tag{1}$$

$$\hat{S}^T \hat{H} \hat{S} = F, \tag{2}$$

where $F_{ij} = \delta_{ij}\omega_j^2$; $M_{ij} = \delta_{ij}m_i$; H is the Hessian matrix; $\hat{H}$ is the mass-weighted Hessian; $\hat{S}$ is the matrix of directional vectors of normal modes in mass-weighted coordinates, which can be transformed into Cartesian coordinates by

$$S = M^{-1/2}\hat{S}. \tag{3}$$

The *j*th column of S, S_j, can be normalized to obtain unitary displacements in Cartesian coordinates

$$\underline{S}_j = \sqrt{\mu_j} S_j \tag{4}$$

where $\mu_j = \left(\left|S_j\right|^2\right)^{-1}$, which is the reduced mass of mode *j*.[42] The normal mode analysis can be done in linear coordinates because the displacements are assumed to be infinitesimal. However, for nonlinear modes such as bends and torsions, non-infinitesimal displacements in linear coordinates along the normal mode lead to unphysical distortions of the geometry, and hence introduce strong, fictitious coupling between modes.[9,41] Therefore, as pointed out in previous studies,[9,41] the distortions along $\underline{S}_j$ have to be done in internal coordinates, instead of Cartesian coordinates

$$x_{i+1} = x_i + (B^{-1})^T q_j \ \Delta x, \tag{5}$$

where x_i is the Cartesian coordinates of step i; B is the well-known Wilson B-matrix; $q_j = B\underline{S}_j$, which is the direction of mode j in internal coordinates; Δx is the step size chosen. Since B is rectangular, no direct inverse can be calculated. However, its generalized inverse can be derived as

$$B^{-1} = (BM^{-1}B^T)^{-1}BM^{-1}. \tag{6}$$

As well documented,[43–46] since internal coordinates are nonlinear, Eq (5) must be solved iteratively to achieve the correct displacements in Cartesian coordinates. Following the recommendations of previous studies,[9,41] the sampling of UM-N was carried out symmetrically for each mode as far as the classical turning points determined by the harmonic frequency

$$\Delta x_j^{max} = \pm 4\sqrt{\frac{\hbar}{\mu_j \omega_j}} \ . \tag{7}$$

As mentioned above in the introduction, an alternative sampling scheme is to sample vibrations and internal rotations separately (UM-VT). This can be achieved by projecting out the internal rotations before the normal mode problem is solved

$$H' = B^T P (B^{-1})^T H (B^{-1}) PB, \tag{8}$$

where P is a projection matrix the diagonal elements of which equal to 0's for the bond torsions and 1's for the other coordinates. With the projected Hessian, H', one can solve for the remaining eigenvectors corresponding to stretches, bends, and out-of-plane motions using Eqs. (1) to (4) and then distort the geometry along these directions with bond torsions intact using

$$x_{i+1} = x_i + (B^{-1})^T P \ \ q_j \ \Delta x. \tag{9}$$

Sampling along each torsional mode can be done similarly with

$$x_{i+1} = x_i + (B^{-1})^T \; q_k \; \Delta\theta, \tag{10}$$

where q_k is a unit vector for displacement along the *k*th bond torsion (i.e. with 0's for all others); $\Delta\theta$ is the step size chosen for the sampling of bond torsions. Hoping to gather more non-local information about the anharmonic PES that might yield improved accuracy for thermodynamic quantities, instead of sampling only the region bound by classical turning points, the sampling of UM-VT was terminated either when the torsional angle displaces by 2π or the energy rises above a cut-off value. The cut-off energy chosen in this work was 0.05 hartree. This value is high enough to ensure the convergence of the thermodynamic quantities of interest in the low and medium temperature range (< 1000K), which will be discussed in detail below.

The discrete data points obtained by either of the two sampling schemes can be used to construct continuous PESs with the aid of cubic spline interpolations. For a set of $N+1$ points sampled for a mode $(E_0, E_1, \ldots, E_N)$, the *i*th piece of the spline is

$$V_i(Q) = a_i + b_i Q + c_i Q^2 + d_i Q^3, \tag{11}$$

where Q is the mass weighted coordinate. For UM-N, Q is set to $\sqrt{\mu}x$ for all the modes; whereas for UM-VT, Q is taken as $\sqrt{\mu}x$ for vibrations and $\sqrt{I}\theta$ for torsions, where I is the reduced moment of inertia of the rotor. In principle, just as the PES of a mode could be affected by the motions of other modes, the reduced moment of inertia of a rotor could be affected by the motions of others. However, under the assumption of uncoupled modes, the reduced moments of inertia can be approximated with the diagonal elements of the internal rotation kinetic energy matrix, which can be derived by the procedures reported by Kilpatrick and Pitzer.[47] The coefficients of Eq. (11) can be determined by restricting V_i to pass through the i^{th} and $(i\text{-}1)^{\text{st}}$ data points

$$V_i(Q_i) = E_i \;\text{ and }\; V_i(Q_{i-1}) = E_{i-1} \tag{12}$$

and requiring the first and second derivatives of the splines to be continuous

$$V_i'(Q_i) = V_{i+1}'(Q_i) \text{ and } V_i''(Q_i) = V_{i+1}''(Q_i). \quad (13)$$

At the endpoints, various boundary conditions can be chosen. For instance, one could either set the first derivatives to zero (clamped conditions) or the second derivatives to zero (natural conditions). In principle, if the cut-off energy employed for sampling is very high, it does not matter which set of boundary conditions are used because the wave function decays to zero before reaching the endpoints. However, to avoid unnecessary computational effort sampling the high energy region, one can instead use a lower cut-off energy and extrapolate the PES beyond the endpoints using quadratic splines

$$V_i(Q) = a_i + b_i Q + c_i Q^2, \quad \forall i \in \{0, N+1\}. \quad (14)$$

The coefficients of Eq. (14) can of course be fully determined by imposing continuity of V, V', and V'' at Q_0 and Q_N. However, for modes with real frequencies, the second derivatives of V at the endpoints must be positive, otherwise Eq. (14) tends to minus infinity as $Q \to \pm\infty$. A reasonable choice is therefore the second derivative of the mode at the origin, which is already available from Eq. (2). Therefore, the boundary conditions of the cubic splines we used were

$$V_1''(Q_0) = V_N''(Q_N) = V''(0). \quad (15)$$

This set of boundary conditions is also a good choice for the PES of a torsional mode since the $V''(0)$ is exactly the second derivative at the end points $Q_0 = 0$ and $Q_N = 2\pi$ (see Text S1 in Supporting Information for the details of how to solve for the coefficients a_i, b_i, c_i, and d_i).

Under the assumption of uncoupled modes, energy levels of the system can be obtained by solving one-dimensional Schrödinger equations for each mode, which can be done variationally with basis functions

$$H_{mn} = \left\langle \varphi_m \middle| -\frac{\hbar^2}{2}\frac{d^2}{dQ^2} + V(Q) \middle| \varphi_n \right\rangle, \tag{16}$$

where H_{mn} is the Hamiltonian matrix element. Since the PES is represented by a collection of splines as described above, the integration of $V(Q)$ has to be done piecewise

$$H_{mn} = \left\langle \varphi_m \middle| -\frac{\hbar^2}{2}\frac{d^2}{dQ^2} \middle| \varphi_n \right\rangle + \sum_i \int_{Q_{i-1}}^{Q_i} \varphi_m V_i \varphi_n dQ. \tag{17}$$

For the vibrational modes, where quadratic potentials are often a reasonable approximation to the 1-D PESs, it is natural to use harmonic oscillator functions as the basis set

$$\varphi_n = \left(\frac{\omega_j}{\pi\hbar}\right)^{\frac{1}{4}} \frac{1}{\sqrt{2^n n!}} H_n\left(\sqrt{\frac{\omega_j}{\hbar}} Q\right) e^{-\omega_j Q^2/2\hbar}. \tag{18}$$

On the other hand, for internal rotations, since the PESs are periodic with period 2π, it is more convenient to use Fourier basis

$$\varphi_0 = \frac{1}{\sqrt{2L}} \text{ and } \varphi_n = \begin{cases} \frac{1}{\sqrt{L}}\cos\left(\frac{n\pi Q}{L}\right) \\ \frac{1}{\sqrt{L}}\sin\left(\frac{n\pi Q}{L}\right) \end{cases}, \ \forall n > 0, \tag{19}$$

where $L = \pi\sqrt{I}$. With harmonic and Fourier basis functions, no numerical integration is needed to compute the matrix elements of Eq. (17) (see Text S2 in Supporting Information for the formulas).

Diagonalization of the Hamilationian matrix yields the energy levels of a mode; and hence the partition function for each mode can be derived as

$$q = \sum_m^M e^{-\beta\epsilon_m} \tag{20}$$

where $\beta = 1/kT$; ϵ_m is the *m*th eigenvalue of the Hamilationian matrix; and *M* is the number of basis functions. The convergence of q and the fundamental anharmonic frequency $\upsilon = (\epsilon_1 - \epsilon_0)/h$ with respect to the number of basis functions were used as variational criteria to truncate the basis. When

they converge ($q^{M+1} - q^M$ and $\upsilon^{M+1} - \upsilon^M$ are below a required tolerance), the partition function was used to calculate thermodynamic properties of interest. Note that for the modes whose PESs are periodic, i.e., internal rotations of UM-VT, eq. (20) has to be divided by the symmetry number of the rotor to derive the correct partition function.

Computational Details:

For UM-N and the vibrations of UM-VT, the step size chosen for sampling was $\sqrt{\hbar/\mu_j\omega_j}$, which is one-fourth of Eq. (7), the distance between the origin and the classical turning point determined by the harmonic frequency. The rationale of making the step size proportional to the classical turning distance is to reduce computational cost by enlarging the spacing between sample points for soft modes. For the torsional modes of UM-VT, to capture the commonly seen three-fold rotational barriers, the largest step size one could use is $\pi/3$. However, to obtain accurate descriptions for the PESs of torsions, a step size of $\pi/18$ was used in this work. As mentioned above, following the methodology of previous studies,[9,41] the sampling of UM-N was carried out symmetrically for each mode to the classical turning points. On the other hand, hoping to achieve a better description of the PES, the sampling of UM-VT was terminated either when the torsional angle has been displaced by 2π or the energy rises more than 0.05 hartree (i.e. about 130 kJ/mol) compared with the reference stationary point. The step sizes and the cut-off energy were examined to ensure satisfactory convergence of thermodynamic calculations, as discussed in the subsection on Convergence.

The reported thermodynamic properties were calculated using the standard equations derived from statistical mechanics (see Text S3 in Supporting Information for the formulas).[48] Geometry optimizations and frequency computations were performed at the ωB97X-D[49,50]/6-311+G(2df,2pd) level of theory, unless noted otherwise. All calculations were done using a development version of the Q-Chem software package.[51]

Results and Discussion:

Partition Functions. Hydrogen peroxide and its isotopologs (D or ^{18}O) were chosen to examine the performance of the HO^{hf} model, UM-N, and UM-VT for evaluation of partition functions as shown in Fig. 1. The benchmarks were the data previously reported by Lynch et al., which were calculated with the PIMC method.[34,35] The PESs of these species were generated using the anharmonic quartic force field reported by Koput et al.,[52] which is the same force field that was used for the PIMC calculations.[34,35]

Figure 1 shows that only about 30% of the partition functions of these molecules can be captured if the HO^{hf} model is used directly, which is consistent with the findings of Truhlar and coworkers.[35] ~~However, a~~A correction is possible, because, as shown in Fig. 2, H_2O_2 and its isotopologs are molecules with a torsion, which has two degenerate minima with nonsuperimposable structures. Since the HO^{hf} model assumes that the PES is a quadratic well, only one minimum is considered, and hence the HO^{hf} partition function is less than 50% of the benchmarks. For H_2O_2 and its isotopologs, one can simply multiply the HO^{hf} partition functions by two to take into account the contributions of both of the minima because they are degenerate. However, since complicated molecules typically have nondegenerate minima, this type of correction is not always applicable.

As shown in Fig. 1, an improvement can be achieved with UM-N, where the PES is described more accurately by splines through data points evaluated along the direction of each normal mode. However, the percentage of the benchmark partition functions that can be captured by UM-N is still under 50%. The reason for this is because for UM-N, the sampling region is defined by the classical harmonic oscillator turning points, which only covers the vicinity of the starting geometry. As shown in Fig. 2, if one initiates the sampling with the structure of the minimum on the left ($\angle HOOH = 112.5°$) and terminates the sampling at the classical turning points, the minimum on the right will not be covered.

One might expect that the problem can be solved by simply expanding the sampling region. However, as shown in Fig. 2, this instead leads to a new problem, namely the PES of the torsion obtained from UM-N with extended sampling was not symmetric. In UM-N, the direction of sampling is determined by the direction of normal modes, which have no clean separation between bond torsions and other stretches and bends. Therefore, when the structure is distorted away from the minimum along the "torsional mode", all the stretches and bends start to deviate from the equilibrium values, which introduces artificial coupling and prevents UM-N from sampling multiple minima of a torsion correctly.

This finding is strong motivation to separate torsions from other modes, which is the reason why we introduce the UM-VT model. Modeling torsions and vibrations separately is not without precedents,[8,37] though the motivation and treatment may vary in literature.[8,37] With UM-VT, as shown in Fig. 2, the symmetry of the torsional PES is restored. Even though the torsional barriers are slightly over estimated comparing with the minimum-energy path because the dihedral angle is varied with all the other coordinates frozen, the PES constructed with UM-VT has two degenerate minima so that its eigenstates include the two conformers of H_2O_2 and its isotopologs. Therefore, on average, UM-VT partition functions of these molecules can capture more than 70% of the benchmark over a broad temperature range (300-2400K), which significantly outperforms the HO^{hf} and UM-N models as shown in Fig. 3.

Following a published strategy[35], the accuracy of the UM-VT partition function can be further improved by correcting the zero-point energy

$$Q_{UM-VT(ZP)} = Q_{UM-VT} \times e^{-\beta(\epsilon_0^{accurate} - \epsilon_0^{UM-VT})} \quad (21)$$

where $\epsilon_0^{accurate}$ is the accurate zero-point energy (available from previous work[35]) and ϵ_0^{UM-VT} is the zero-point energy calculated using the UM-VT model. As shown in Fig. 1 and Fig. 3, the zero-point corrected UM-VT partition function captures more than 90% of the benchmark in the low and medium temperature range (< 1000K). Unfortunately, this correction cannot be applied universally because a

zero-point energy that is sufficiently accurate for this purpose is rarely available. After all, even an 0.1 kcal/mol error in the zero-point energy will lead to a 15% underestimation of the partition function at 300K. However, the good agreement between the zero-point corrected UM-VT partition function and the benchmark suggests that the number and spacing of energy levels are adequately captured by the UM-VT model. In the following subsection, we shall explore whether or not heat capacities, standard entropies, and enthalpy increments calculated with the UM-VT model also agree well with the benchmarks.

Heat capacities, Entropies and Enthalpies. Further examination of the methods were carried out for larger molecules. As listed in Table 1, heat capacities for nine selected alkanes ranging in size from C5 to C8 were calculated with HO^{hf}, UM-N, and UM-VT. The benchmarks chosen are the ideal gas heat capacities obtained by measuring heat capacities at two or more pressures and extrapolating linearly to zero pressure.[53–57] As shown in Fig. 4, because of the absence of ~~–~~anharmonic effects, all of the heat capacities calculated with the HO^{hf} model are underestimated. The UM-N heat capacities are slightly more accurate than those of the HO^{hf} model since the UM-N model takes local anharmonicities into account. ~~However, t~~The improvements were not very significant because, as discussed above, the UM-N sampling scheme cannot handle internal rotors properly. Separating torsions and vibrations helps to remedy the problem. As listed in Table 1, the RMS error is reduced to less than 1 cal mol^{-1} K^{-1} with the UM-VT model. The UM-VT heat capacities agree well with the experimental values and no systematic error is observed, suggesting that the energy levels calculated with UM-VT are sufficiently accurate to obtain correct thermodynamic properties, which is consistent with what we observed for the H_2O_2 partition functions. This also indicates that the large basis ωB97X-D DFT calculations are adequately describing the electronic potential energy surface of these alkanes.

In addition to heat capacities, we also examined the performance of these methods for entropy and enthalpy calculations for C2 to C8 branched and linear alkanes and species with different moieties

as listed in Table 2 and Table 3. Because experimentally measured entropies and enthalpies are very rare, the HO^{hf}, UM-N, and UM-VT values are compared with the data collected by NIST/TRC,[58,59] which were mostly calculated using statistical mechanics based on spectral data, frequently with internal rotor corrections but without considering anharmonicity or coupling effects. As listed in Table 2, most of the entropies are significantly underestimated with the HO^{hf} model, especially for long-chain alkanes, because of the inaccurate treatments for the torsional modes. Normal octane, the molecule with the highest number of internal rotors deviates the most from the reference value. As shown in Fig. 5, the UM-N results are slightly more accurate compared to the HO^{hf} model, which is similar to what we observed for the heat capacity calculations. Separating torsions and vibrations significantly improves the accuracy. For instance, for n-octane, the error is reduced to less than ~~1~~ 2 cal mol^{-1} K^{-1} with the UM-VT model. The accuracy of the other molecules ~~are~~ is also improved systematically with UM-VT. The overall performance of the methods for entropy calculations is summarized in Fig. 6. Over the 300-1000K temperature range, the RMS error is about ~~6~~5 ~~9~~ 6.5 cal mol^{-1} K^{-1} using the HO^{hf} model. The UM-N RMS errors are slightly lower, at around ~~5~~4 ~~7~~ 5.5 cal mol^{-1} K^{-1}. By contrast, the UM-VT RMS error is about 1-2 cal mol^{-1} K^{-1}, which is significantly lower than the HO^{hf} and UM-N RMS errors, and hence validates the superior accuracy of the UM-VT calculated entropies for molecules with internal rotors. ~~We note that for the internal rotors with only one minimum or multiple minima which are superimposable, the HO^{hf} model can perform quite accurately, such as for the ethane case. No distinct configuration is omitted from the HO^{hf} model in this case.~~

The performance of these methods for enthalpy calculations was examined from 0K to higher temperatures. As shown in Fig. 7 and Table 3, all of the UM-VT enthalpies agree well with the reference at 298K. While their performance is not as good as UM-VT, most of the enthalpies calculated with the UM-N and HO^{hf} models also lie within the ± 1 kcal/mol error bar despite the limitations of these two models. At higher temperatures, as shown in Fig. 8, the UM-VT RMS error is more significantly

Formatted: Font: (Default) Times New Roman, Font color: Black, Pattern: Clear

Formatted: Font: 12 pt, Not Italic, Font color: Black, Pattern: Clear

Formatted: Font: (Default) Times New Roman, Font color: Black, Pattern: Clear

reduced relative to the HO^{hf} and UM-N models, which indicates that taking internal rotors into account does improve the accuracy. The enthalpy is not very sensitive to the choice of the model because it is based on the first derivative of the logarithm of the partition function

$$H = RT^2 \frac{\partial ln(Q)}{\partial T} + RT \quad (22)$$

The logarithm inherently deemphasizes the differences in the partition function, and the derivative wipes out the contribution of degenerate conformers (as discussed earlier for H_2O_2, where the HO^{hf} partition function should be corrected by a factor of two). Therefore, for enthalpy calculations, even the uncorrected HO^{hf} model can be reasonably accurate. By contrast, a proper correction for degenerate conformers is essential for reliable entropies, because the entropy depends directly on the logarithm of the partition function:

$$S = RT \frac{\partial ln(Q)}{\partial T} + Rln(Q) \quad (23)$$

Thus the entropy is affected by the constant scaling of the partition function. The calculation of the heat capacity is more sensitive to the accuracy of the energy levels than is the enthalpy, since the heat capacity is the derivative of the enthalpy with respect to temperature, which incurs a second derivative of the partition function. Therefore, the enthalpies are less sensitive to the choice of the model than either the entropy or the heat capacity.

Convergence. The success of the UM-VT model discussed above was achieved using the ωB97X-D/6-311+G(2df,2pd) level of electronic structure theory. However, the most demanding real-world problems involve larger systems for which frequency calculations using a range-separated hybrid GGA with valence triple-ζ basis sets including f-functions are computationally very costly or perhaps not even feasible. In light of this, we examined the performance of the UM-VT model with B97-D^{60}/6-31G*, a much less computationally demanding level of electronic structure theory (more than 50 times faster, typically). The B97-D/6-31G* tests were carried out for heat capacities listed in Table 1 since, as discussed above, heat capacity is more sensitive to the energy levels and has good experimental

Formatted: Indent: First line: 0"

benchmarks. We found that, as listed in Table 4, the statistical errors do not significantly increase if ωB97X-D/6-311+G(2df,2pd) is replaced by B97-D/6-31G*. Therefore, from the perspective of computational cost, B97-D/6-31G* is an attractive alternative if ωB97X-D/6-311+G(2df,2pd) is not feasible for larger systems of interest. Just as optimized molecular structures are well-known to depend more weakly on basis set and correlation treatment than relative energies, it is reasonable that the treatment of local vibrations may not be overly sensitive to the level of theory employed.

A last remark should be made on the convergence of the UM-VT calculations with respect to the step size and the cut-off energy for sampling. We recomputed the heat capacities listed in Table 1 after doubling the cut-off energy and halving the step sizes for torsions and vibrations, respectively. As listed in Table 4, making more conservative (and computationally expensive) choices for these parameters did not affect the accuracy of the model, suggesting that the original step size and cut-off energy was adequate to achieve converged calculations.

Conclusions:

The purpose of this work was to explore approaches that go beyond the standard harmonic oscillator model with harmonic frequencies (HO^{hf}) for nuclear motion without changing the computational cost scaling (only increasing the prefactor). To this end, partition functions, heat capacities, entropies, and enthalpies of molecules with internal rotors were calculated using uncoupled mode (UM) approximations, where the full-dimensional PESs of internal motions were treated as a collection of independent one-dimensional potentials. The accuracy of this approach depends critically on how the one-dimensional potentials are determined. The HO^{hf} model, which assumes that the PESs of all modes are quadratic, can capture only about 30% of the partition functions of hydrogen peroxide and its isotopologs at 300K because there are two degenerate minima with nonsuperimposable structures on the torsional coordinate, whereas only one of them is taken into account if the PES is assumed to be quadratic.

Limitations of the HO^{hf} model are not strongly evident in the calculations of enthalpies since, for a selected test set of linear and branched C1 to C8 alkanes and species with different moieties, the RMS error of the enthalpy changes from 0 to 298K calculated by the HO^{hf} model is less than 1 kcal/mol. However, as is well-known, the HO^{hf} model strongly limits the accuracy that can be achieved for entropy calculations. For the same test set, the RMS error of standard entropies calculated by the HO^{hf} model is ~~6.33~~4.74 cal mol^{-1} K^{-1} at 298K. As the temperature rises, the error further increases. Systematic error is also observed for the HO^{hf} heat capacities.

More realistic representations of one-dimensional PESs help to alleviate the problem. Our first attempt was to reconstruct the PESs by interpolating energies of geometries distorted along each normal mode with cubic splines (the UM-N model). To obtain energy levels of these PESs, a computational protocol solving one-dimensional Schrödinger equations with potentials represented by cubic splines was established. However, it was found that though UM-N successfully takes local anharmonicities into account, it cannot recover qualitatively correct (i.e., periodic) PESs for bond torsions. Therefore, the improvements in calculations of thermodynamic properties using UM-N were quite limited relative to the basic HO^{hf} model.

Significant improvements were achieved by constructing the 1D PESs of torsions and vibrations separately (UM-VT). The PESs were still constructed by interpolating energies of geometries distorted along each mode with cubic splines. However, instead of using normal mode directions, the directions of torsional and vibrational modes were determined by the torsional coordinates and the eigenvectors of the Hessian with torsional modes projected out, respectively. On average, UM-VT captures more than 70% of the partition functions of hydrogen peroxide and its isotopologs between 300K and 2400K. The UM-VT heat capacities agree with the experimental values to within a RMS error of 0.~~73~~ 78 cal mol^{-1} K^{-1} for nine selected alkanes ranging from C5 to C8. For the calculations of standard entropies of branched and straight chain alkanes and other standard organic species, the UM-VT RMS error is about

1-2 cal mol^{-1} K^{-1} over the temperature range of 300 K to 1000 K, which is less than one-third of the RMS error of the HO^{hf} model for the same test set. The UM-VT model also improves the accuracy in enthalpy calculations though the error of the HO^{hf} model for our test set was quite small to begin with, particularly at lower temperatures.

Acknowledgement:

This work was supported by a grant from Chevron Energy Technology. MHG acknowledges support from the U.S. Department of Energy under Contract No. DE-AC02-05CH11231. We acknowledge very helpful comments from an anonymous reviewer, including the suggestion to compare against experimental heat capacity measurements.

Supporting Information Available

Additional information as noted in the text, including formulas for solving for the coefficients of cubic splines ~~and~~, anharmonic Hamiltonian matrix elements, and equations for thermodynamic calculations. This information is available free of charge via the Internet at http://pubs.acs.org/.

References:

(1) Bell, A. T.; Head-Gordon, M. *Annu. Rev. Chem. Biomol. Eng.* **2011**, *2*, 453–477.
(2) Grimme, S. *Chem. – Eur. J.* **2012**, *18*, 9955–9964.
(3) Li, Y.-P.; Head-Gordon, M.; Bell, A. T. *ACS Catal.* **2014**, *4*, 1537–1545.
(4) Li, Y.-P.; Head-Gordon, M.; Bell, A. T. *J. Phys. Chem. C* **2014**, *118*, 22090–22095.
(5) Li, Y.-P.; Gomes, J.; Mallikarjun Sharada, S.; Bell, A. T.; Head-Gordon, M. *J. Phys. Chem. C* **2015**, *119*, 1840–1850.
(6) Mardirossian, N.; Head-Gordon, M. *Phys. Chem. Chem. Phys.* **2014**, *16*, 9904–9924.
(7) Ruscic, B. *Int. J. Quantum Chem.* **2014**, *114*, 1097–1101.
(8) Ayala, P. Y.; Schlegel, H. B. *J. Chem. Phys.* **1998**, *108*, 2314–2325.
(9) Piccini, G.; Sauer, J. *J. Chem. Theory Comput.* **2014**, *10*, 2479–2487.
(10) Piccini, G.; Alessio, M.; Sauer, J.; Zhi, Y.; Liu, Y.; Kolvenbach, R.; Jentys, A.; Lercher, J. A. *J. Phys. Chem. C* **2015**, *119*, 6128–6137.
(11) Piccini, G.; Sauer, J. *J. Chem. Theory Comput.* **2013**, *9*, 5038–5045.
(12) Scott, A. P.; Radom, L. *J. Phys. Chem.* **1996**, *100*, 16502–16513.
(13) Andersson, M. P.; Uvdal, P. *J. Phys. Chem. A* **2005**, *109*, 2937–2941.
(14) Martin, J. M. L.; Lee, T. J. *Chem. Phys. Lett.* **1996**, *258*, 129–135.
(15) Lee, T. J.; Martin, J. M. L.; Taylor, P. R. *J. Chem. Phys.* **1995**, *102*, 254–261.
(16) Martin, J. M. L.; Lee, T. J.; Taylor, P. R. *J. Chem. Phys.* **1992**, *97*, 8361–8371.
(17) Dateo, C. E.; Lee, T. J.; Schwenke, D. W. *J. Chem. Phys.* **1994**, *101*, 5853–5859.
(18) Schuurman, M. S.; Allen, W. D.; Schaefer, H. F. *J. Comput. Chem.* **2005**, *26*, 1106–1112.
(19) Bowman, J. M. *J. Chem. Phys.* **1978**, *68*, 608–610.
(20) Gerber, R.; Ratner, M. *Adv. Chem. Phys.* **1988**, *70*, 97–132.
(21) Bowman, J. M. *Acc. Chem. Res.* **1986**, *19*, 202–208.
(22) Barone, V. *J. Chem. Phys.* **2005**, *122*, 014108.
(23) Neugebauer, J.; Hess, B. A. *J. Chem. Phys.* **2003**, *118*, 7215–7225.
(24) Adel, A.; Dennison, D. M. *Phys. Rev.* **1933**, *43*, 716–723.
(25) Nielsen, H. H. *Phys. Rev.* **1941**, *60*, 794–810.
(26) Wilson, E. B.; Howard, J. B. *J. Chem. Phys.* **1936**, *4*, 260–268.
(27) Bowman, J. M.; Christoffel, K.; Tobin, F. *J. Phys. Chem.* **1979**, *83*, 905–912.
(28) Carter, S.; Bowman, J. M.; Handy, N. C. *Theor. Chem. Acc.* **1998**, *100*, 191–198.
(29) Christoffel, K. M.; Bowman, J. M. *Chem. Phys. Lett.* **1982**, *85*, 220–224.
(30) Whitehead, R. J.; Handy, N. C. *J. Mol. Spectrosc.* **1975**, *55*, 356–373.
(31) Rauhut, G.; Knizia, G.; Werner, H.-J. *J. Chem. Phys.* **2009**, *130*, 054105.
(32) Besler, B. H.; Scuseria, G. E.; Scheiner, A. C.; Schaefer, H. F. *J. Chem. Phys.* **1988**, *89*, 360–366.
(33) Christiansen, O. *J. Chem. Phys.* **2004**, *120*, 2149–2159.
(34) Lynch, V. A.; Mielke, S. L.; Truhlar, D. G. *J. Chem. Phys.* **2004**, *121*, 5148–5162.
(35) Lynch, V. A.; Mielke, S. L.; Truhlar, D. G. *J. Phys. Chem. A* **2005**, *109*, 10092–10099.
(36) Zheng, J.; Truhlar, D. G. *J. Chem. Theory Comput.* **2013**, *9*, 2875–2881.
(37) Ellingson, B. A.; Lynch, V. A.; Mielke, S. L.; Truhlar, D. G. *J. Chem. Phys.* **2006**, *125*, 084305.
(38) Pitzer, K. S.; Gwinn, W. D. *J. Chem. Phys.* **1942**, *10*, 428–440.
(39) Nagy, B.; Csontos, B.; Csontos, J.; Szakács, P.; Kállay, M. *J. Phys. Chem. A* **2014**, *118*, 4824–4836.
(40) Wang, H.; Castillo, Á.; Bozzelli, J. W. *J. Phys. Chem. A* **2015**, *119*, 8202–8215.
(41) Njegic, B.; Gordon, M. S. *J. Chem. Phys.* **2008**, *129*, 164107.
(42) Ochterski, J. W. Vibrational Analysis in Gaussian http://www.gaussian.com/g_whitepap/vib.htm (accessed Apr 17, 2016).

(43) Baker, J.; Kinghorn, D.; Pulay, P. *J. Chem. Phys.* **1999**, *110*, 4986–4991.
(44) Baker, J.; Pulay, P. *J. Chem. Phys.* **1996**, *105*, 11100–11107.
(45) Bakken, V.; Helgaker, T. *J. Chem. Phys.* **2002**, *117*, 9160–9174.
(46) Baker, J.; Kessi, A.; Delley, B. *J. Chem. Phys.* **1996**, *105*, 192–212.
(47) Kilpatrick, J. E.; Pitzer, K. S. *J. Chem. Phys.* **1949**, *17*, 1064–1075.
(48) Irikura, K. K.; Frurip, D. J. *Computational Thermochemistry : Prediction and Estimation of Molecular Thermodynamics*; ACS symposium series: 677; American Chemical Society, 1998; Chapter 22, pp 402-418.
(49) Chai, J.-D.; Head-Gordon, M. *Phys. Chem. Chem. Phys.* **2008**, *10*, 6615–6620.
(50) Chai, J.-D.; Head-Gordon, M. *J. Chem. Phys.* **2008**, *128*, 084106–084115.
(51) Shao, Y.; Gan, Z.; Epifanovsky, E.; Gilbert, A. T. B.; Wormit, M.; Kussmann, J.; Lange, A. W.; Behn, A.; Deng, J.; Feng, X.; Ghosh, D.; Goldey, M.; Horn, P. R.; Jacobson, L. D.; Kaliman, I.; Khaliullin, R. Z.; Kuś, T.; Landau, A.; Liu, J.; Proynov, E. I.; Rhee, Y. M.; Richard, R. M.; Rohrdanz, M. A.; Steele, R. P.; Sundstrom, E. J.; Woodcock, H. L.; Zimmerman, P. M.; Zuev, D.; Albrecht, B.; Alguire, E.; Austin, B.; Beran, G. J. O.; Bernard, Y. A.; Berquist, E.; Brandhorst, K.; Bravaya, K. B.; Brown, S. T.; Casanova, D.; Chang, C.-M.; Chen, Y.; Chien, S. H.; Closser, K. D.; Crittenden, D. L.; Diedenhofen, M.; DiStasio, R. A.; Do, H.; Dutoi, A. D.; Edgar, R. G.; Fatehi, S.; Fusti-Molnar, L.; Ghysels, A.; Golubeva-Zadorozhnaya, A.; Gomes, J.; Hanson-Heine, M. W. D.; Harbach, P. H. P.; Hauser, A. W.; Hohenstein, E. G.; Holden, Z. C.; Jagau, T.-C.; Ji, H.; Kaduk, B.; Khistyaev, K.; Kim, J.; Kim, J.; King, R. A.; Klunzinger, P.; Kosenkov, D.; Kowalczyk, T.; Krauter, C. M.; Lao, K. U.; Laurent, A. D.; Lawler, K. V.; Levchenko, S. V.; Lin, C. Y.; Liu, F.; Livshits, E.; Lochan, R. C.; Luenser, A.; Manohar, P.; Manzer, S. F.; Mao, S.-P.; Mardirossian, N.; Marenich, A. V.; Maurer, S. A.; Mayhall, N. J.; Neuscamman, E.; Oana, C. M.; Olivares-Amaya, R.; O'Neill, D. P.; Parkhill, J. A.; Perrine, T. M.; Peverati, R.; Prociuk, A.; Rehn, D. R.; Rosta, E.; Russ, N. J.; Sharada, S. M.; Sharma, S.; Small, D. W.; Sodt, A.; Stein, T.; Stück, D.; Su, Y.-C.; Thom, A. J. W.; Tsuchimochi, T.; Vanovschi, V.; Vogt, L.; Vydrov, O.; Wang, T.; Watson, M. A.; Wenzel, J.; White, A.; Williams, C. F.; Yang, J.; Yeganeh, S.; Yost, S. R.; You, Z.-Q.; Zhang, I. Y.; Zhang, X.; Zhao, Y.; Brooks, B. R.; Chan, G. K. L.; Chipman, D. M.; Cramer, C. J.; Goddard, W. A.; Gordon, M. S.; Hehre, W. J.; Klamt, A.; Schaefer, H. F.; Schmidt, M. W.; Sherrill, C. D.; Truhlar, D. G.; Warshel, A.; Xu, X.; Aspuru-Guzik, A.; Baer, R.; Bell, A. T.; Besley, N. A.; Chai, J.-D.; Dreuw, A.; Dunietz, B. D.; Furlani, T. R.; Gwaltney, S. R.; Hsu, C.-P.; Jung, Y.; Kong, J.; Lambrecht, D. S.; Liang, W.; Ochsenfeld, C.; Rassolov, V. A.; Slipchenko, L. V.; Subotnik, J. E.; Van Voorhis, T.; Herbert, J. M.; Krylov, A. I.; Gill, P. M. W.; Head-Gordon, M. *Mol. Phys.* **2015**, *113*, 184–215.
(52) Koput, J.; Carter, S.; Handy, N. C. *J. Phys. Chem. A* **1998**, *102*, 6325–6330.
(53) Scott, D. W.; McCullough, J. P.; Williamson, K. D.; Waddington, G. *J. Am. Chem. Soc.* **1951**, *73*, 1707–1712.
(54) Waddington, G.; Douslin, D. R. *J. Am. Chem. Soc.* **1947**, *69*, 2275–2279.
(55) Waddington, G.; Smith, J. C.; Scott, D. W.; Huffman, H. M. *J. Am. Chem. Soc.* **1949**, *71*, 3902–3906.
(56) Waddington, G.; Todd, S. S.; Huffman, H. M. *J. Am. Chem. Soc.* **1947**, *69*, 22–30.
(57) Barrow, G. M. *J. Am. Chem. Soc.* **1951**, *73*, 1824–1826.
(58) *NIST/TRC Table Database (CD-ROM)*; Thermodynamics Research Center, 2004.
(59) Frenkel′, M. L. *Thermodynamics of Organic Compounds in the Gas State*; TRC data series; Thermodynamics Research Center, 1994; p 395, p 460.
(60) Grimme, S. *J. Comput. Chem.* **2006**, *27*, 1787–1799.

Table 1. Heat capacities of selected molecules (cal mol^{-1} K^{-1}).

	Temperature (K)	Expt	HO^{hf}	UM-N	UM-VT
Isopentane	317.2	29.95 [a]	28.27	28.23	29.97
	358.2	33.25 [a]	31.47	31.44	33.04
	402.3	36.72 [a]	34.94	34.91	36.29
	449.2	40.24 [a]	38.53	38.50	39.59
	487.1	42.93 [a]	41.29	41.27	42.11
n-Hexane	333.9	37.35 [b]	34.41	34.62	36.86
	365.2	40.22 [b]	37.36	37.57	39.54
	398.9	43.30 [b]	40.55	40.77	42.42
	433.7	46.39 [b]	43.79	44.01	45.33
	468.9	49.46 [b]	46.97	47.18	48.17
2,2-Dimethylbutane	341.6	38.10 [b]	34.25	37.19	39.24
	353.2	39.25 [b]	35.42	38.30	40.33
	376.1	41.50 [b]	37.71	40.48	42.45
	412.4	44.95 [b]	41.28	43.87	45.73
	449.4	48.33 [b]	44.80	47.19	48.92
2,3-Dimethylbutane	341.6	37.78 [c]	36.16	35.93	38.91
	371.2	40.69 [c]	38.95	38.72	41.58
	402.3	43.63 [c]	41.86	41.63	44.32
	436.0	46.73 [c]	44.94	44.71	47.17
	471.2	49.77 [c]	48.05	47.81	50.00
2-Methylpentane	325.1	36.77 [c]	34.08	34.10	36.51
	362.2	40.30 [c]	37.56	37.59	39.79
	402.3	44.08 [c]	41.34	41.38	43.26
	436.2	47.14 [c]	44.47	44.51	46.10
	471.2	50.16 [c]	47.58	47.63	48.90
3-Methylpentane	332.1	36.88 [c]	34.72	34.58	37.54
	367.6	40.25 [c]	38.07	37.91	40.54
	402.4	43.43 [c]	41.35	41.17	43.46
	436.2	46.52 [c]	44.47	44.28	46.23
	471.2	49.55 [c]	47.58	47.39	48.99
n-Heptane	357.1	45.77 [d]	41.96	42.28	46.18
	373.2	47.51 [d]	43.74	44.02	47.66
	400.4	50.37 [d]	46.75	46.99	50.18
	434.4	53.85 [d]	50.44	50.62	53.29
	466.1	57.00 [d]	53.78	53.91	56.12
2,2,3-Trimethylbutane	328.8	42.74 [d]	41.20	40.69	44.11
	348.9	45.09 [d]	43.41	42.90	46.22
	369.2	47.39 [d]	45.64	45.14	48.33

	400.4	50.92 [d]	49.03	48.52	51.49
	434.3	54.54 [d]	52.61	52.09	54.79
	461.8	57.36 [d]	55.42	54.90	57.36
n-Octane	405.7	58.00 [e]	53.86	54.17	57.51
	462.5	64.70 [e]	60.79	61.01	63.38
	522.7	70.60 [e]	67.65	67.77	69.24
MSE			-2.57	-2.31	-0.05
MAE			2.57	2.31	0.68
RMS			2.69	2.41	0.78

[a] Ref [53]
[b] Ref [54]
[c] Ref [55]
[d] Ref [56]
[e] Ref [57]

Table 2. Standard entropies (298.15K, 1bar) of selected molecules (cal mol^{-1} K^{-1}).

	Ref	HO^{hf}	UM-N	UM-VT
Ethane	54.79 [a]	52.90	54.79	54.75
Propane	64.61 [a]	63.31	64.17	64.57
n-Butane	74.10 [a]	72.21	71.95	74.21
Isobutane	70.63 [a]	69.71	69.75	70.22
n-Pentane	83.55 [a]	80.26	79.46	83.56
Isopentane	82.16 [a]	79.68	79.28	81.51
Neopentane	73.14 [a]	71.66	72.77	73.18
n-Hexane	92.94 [a]	86.87	86.95	93.49
2,2-Dimethylbutane	85.66 [a]	78.47	83.83	84.97
2,3-Dimethylbutane	87.46 [a]	82.86	83.77	85.17
2-Methylpentane	91.06 [a]	86.75	86.79	90.56
3-Methylpentane	91.54 [a]	86.41	86.42	90.54
n-Heptane	102.32 [a]	91.53	93.56	102.88
2,2-Dimethylpentane	93.86 [a]	94.89	91.88	92.71
2,3-Dimethylpentane	99.11 [a]	94.33	92.51	94.72
2,4-Dimethylpentane	94.89 [a]	90.36	90.66	92.80
3,3-Dimethylpentane	95.20 [a]	89.62	89.81	93.66
3-Ethylpentane	98.37 [a]	92.45	92.33	96.25
2-Methylhexane	100.50 [a]	94.73	94.28	100.48
3-Methylhexane	101.84 [a]	95.95	94.37	99.94
2,2,3-Trimethylbutane	91.63 [a]	92.29	90.24	90.06
n-Octane	111.70 [a]	97.75	101.36	113.51
1-Butene	73.58 [a]	70.05	71.09	73.36
1,3-Butadiene	66.63 [a]	64.34	66.05	66.05
Ethyl Methyl Ether	73.91 [a]	72.34	72.36	73.07
Ethanol	67.07 [a]	63.88	65.18	66.41
Propionaldehyde	72.75 [a]	69.66	70.89	72.73
2-Butanone	81.12 [a]	76.27	78.83	80.63
Acetic Acid	67.75 [a]	67.35	68.37	68.06
Propylamine	77.78 [a]	71.96	73.13	76.63
1-Nitropropane	83.80 [a]	82.01	82.35	84.68
1-Fluoropropane	72.85 [a]	70.33	71.14	73.11
1-Chloropropane	75.43 [a]	72.88	73.64	75.54
1-Bromopropane	79.07 [b]	75.32	76.25	78.08
Ethyl Methyl Sulfide	79.64 [a]	75.34	77.19	79.41
Methyl Disulfide	80.16 [a]	75.36	78.12	80.12
Ethanethiol	70.79 [a]	67.95	69.16	71.01
Ethylene Glycol	72.61 [b]	68.11	71.33	74.56
Acrylic Acid	73.54 [a]	71.04	71.49	72.18
MSE		-3.85	-3.13	-0.51
MAE		3.94	3.16	0.87
RMS		4.74	3.97	1.24

[a] Ref [58]
[b] Ref [59]

Table 3. Enthalpies H(298.15K)-H(0K) of selected molecules (kcal/mol).

	Ref	HO[hf]	UM-N	UM-VT
Ethane	2.84 [a]	2.76	2.84	2.83
Propane	3.52 [a]	3.32	3.43	3.53
n-Butane	4.61 [a]	4.26	4.24	4.61
Isobutane	4.29 [a]	4.14	4.14	4.28
n-Pentane	5.78 [a]	5.09	5.06	5.65
Isopentane	5.26 [a]	4.96	4.94	5.38
Neopentane	5.54 [a]	4.76	4.91	5.04
n-Hexane	6.86 [a]	5.85	5.88	6.78
2,2-Dimethylbutane	6.01 [a]	4.85	5.66	6.41
2,3-Dimethylbutane	5.85 [a]	5.72	5.67	6.31
2-Methylpentane	6.29 [a]	5.76	5.77	6.42
3-Methylpentane	6.23 [a]	5.75	5.74	6.57
n-Heptane	7.94 [a]	6.47	6.69	8.13
2,2-Dimethylpentane	6.98 [a]	6.61	6.49	7.13
2,3-Dimethylpentane	6.77 [a]	6.64	6.51	6.99
2,4-Dimethylpentane	7.00 [a]	6.46	6.50	6.96
3,3-Dimethylpentane	6.94 [a]	6.49	6.44	7.30
3-Ethylpentane	7.50 [a]	6.65	6.62	7.49
2-Methylhexane	7.39 [a]	6.61	6.61	7.62
3-Methylhexane	7.26 [a]	6.71	6.60	7.63
2,2,3-Trimethylbutane	6.69 [a]	6.51	6.36	7.26
n-Octane	9.03 [a]	7.34	7.57	9.33
1-Butene	4.09 [a]	3.79	3.90	4.09
1,3-Butadiene	3.62 [a]	3.45	3.49	3.52
Ethyl Methyl Ether	4.42 [a]	4.08	4.10	4.55
Ethanol	3.41 [a]	3.20	3.41	3.63
Propionaldehyde	4.18 [a]	3.67	3.78	4.13
2-Butanone	5.01 [a]	4.47	4.66	5.17
Acetic Acid	3.25 [a]	3.35	3.40	3.41
Propylamine	4.27 [a]	4.07	4.24	4.68
1-Nitropropane	4.66 [a]	4.77	4.79	5.05
1-Fluoropropane	3.75 [a]	3.75	3.85	3.88
1-Chloropropane	3.85 [a]	3.90	3.99	4.16
1-Bromopropane	4.10 [b]	3.96	4.07	4.28
Ethyl Methyl Sulfide	4.57 [a]	4.31	4.50	5.00
Methyl Disulfide	4.77 [a]	4.50	4.63	5.30
Ethanethiol	3.71 [a]	3.50	3.68	3.84
Ethylene Glycol	3.96 [b]	3.90	4.14	4.69
Acrylic Acid	3.90 [a]	3.68	3.72	3.87
MSE		-0.41	-0.33	0.17
MAE		0.42	0.37	0.22
RMS		0.57	0.50	0.29

[a] Ref [58]
[b] Ref [59]

Table 4. Statistical errors of heat capacities listed in Table 1 calculated by UM-VT.

Level of theory	Step size		E cut-off (hartree)	MSE (cal mol^{-1} K^{-1})	MAE (cal mol^{-1} K^{-1})	RMS (cal mol^{-1} K^{-1})
	Torsion	Vibration				
ωB97X-D/6-311+G(2df,2pd)	$\pi/18$	$\sqrt{\hbar/\mu_j\omega_j}$	0.05	-0.05	0.68	0.78
B97-D/6-31G*	$\pi/18$	$\sqrt{\hbar/\mu_j\omega_j}$	0.05	0.49	0.70	0.92
B97-D/6-31G*	$\pi/36$	$\sqrt{\hbar/\mu_j\omega_j}$	0.05	0.49	0.70	0.92
B97-D/6-31G*	$\pi/18$	$\frac{1}{2}\sqrt{\hbar/\mu_j\omega_j}$	0.05	0.49	0.70	0.92
B97-D/6-31G*	$\pi/18$	$\sqrt{\hbar/\mu_j\omega_j}$	0.1	0.49	0.70	0.92

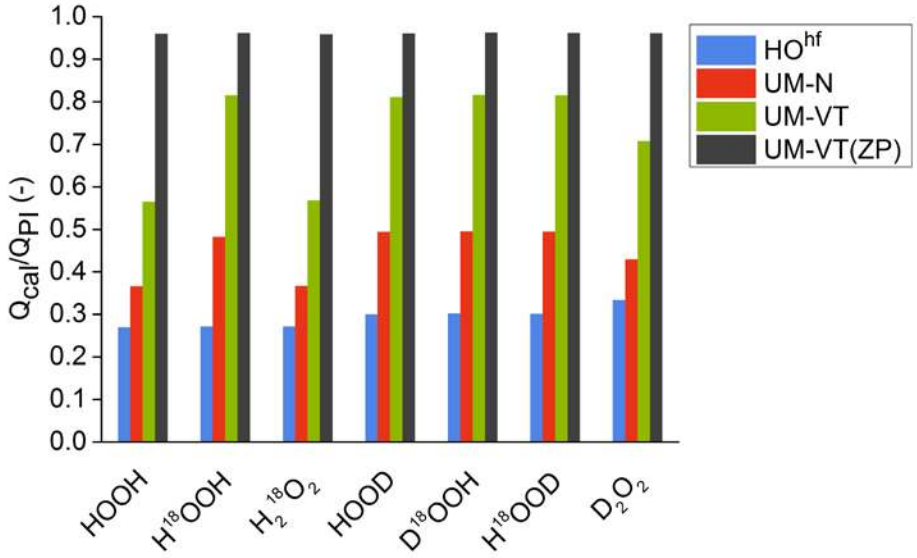

Figure 1. Ratios of the partition functions calculated by HO^{hf}, UM-N, UM-VT, and UM-VT(ZP) to the partition functions calculated by the path integral method at 300K. These ratios represent the percentages of the partition functions that can be captured by the models.

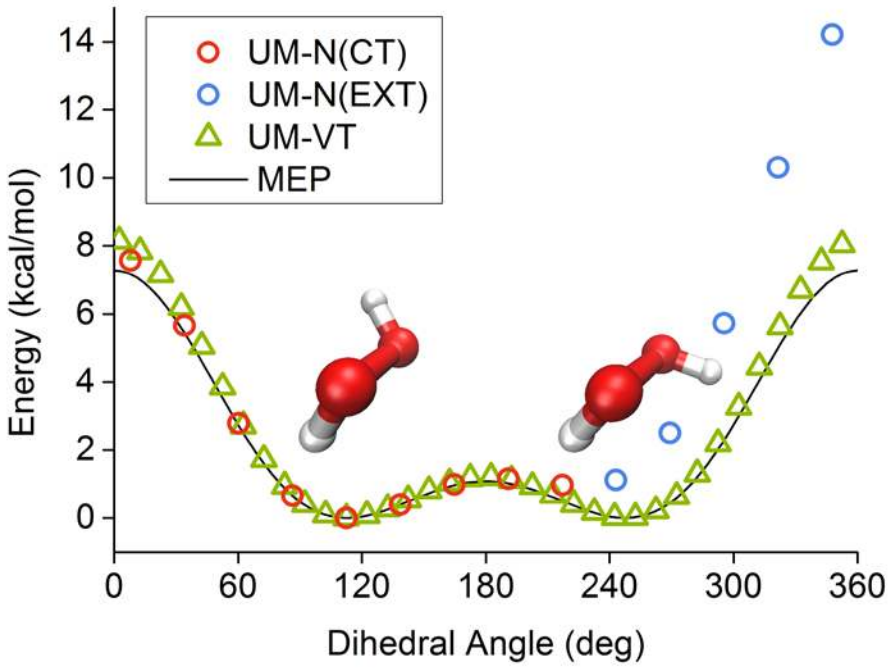

Figure 2. The potential energy surface of the torsion of H_2O_2. The black curve is the minimum-energy path. The circles are the data sampled with UM-N. Those shown in red are within the sampling region defined by the classical turning points (CT). Extending the sampling region of UM-N yields the blue circles (EXT). The green triangles are the data sampled with UM-VT.

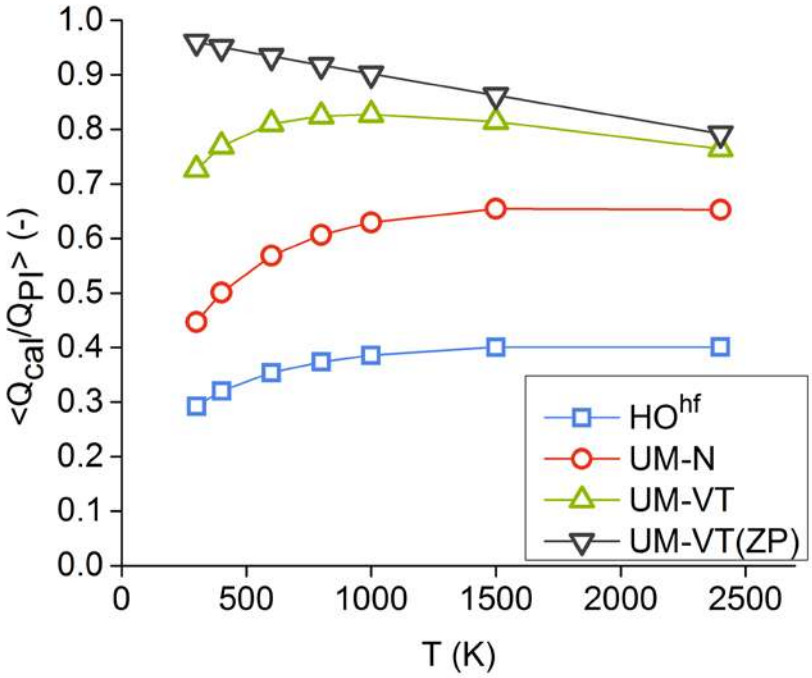

Figure 3. Average of the ratios of partition functions (Q_{cal}/Q_{PI}) over HOOH, $H^{18}OOH$, $H_2{}^{18}O_2$, HOOD, $D^{18}OOH$, $H^{18}OOD$, and D_2O_2.

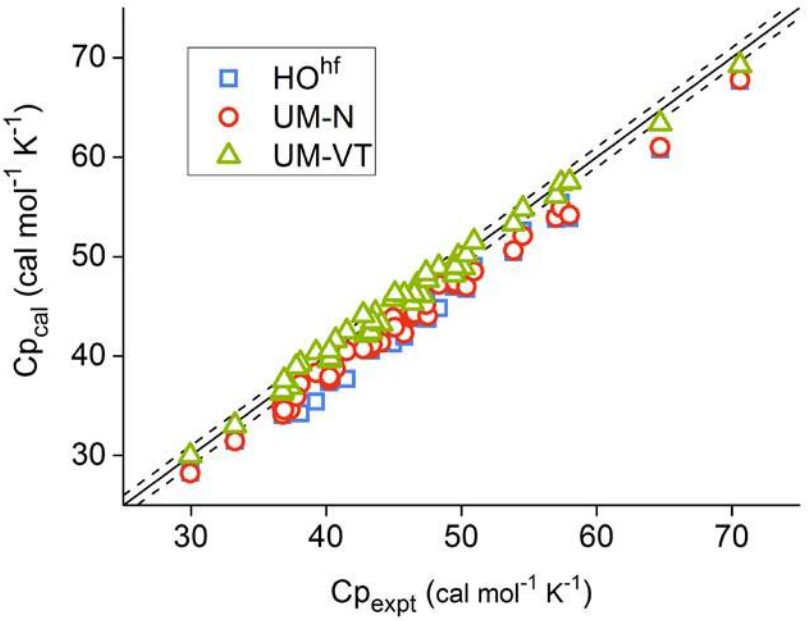

Figure 4. Parity plot of the heat capacities listed in Table 1. An error bar of ± 1 cal mol^{-1} K^{-1} is shown by the dashed lines.

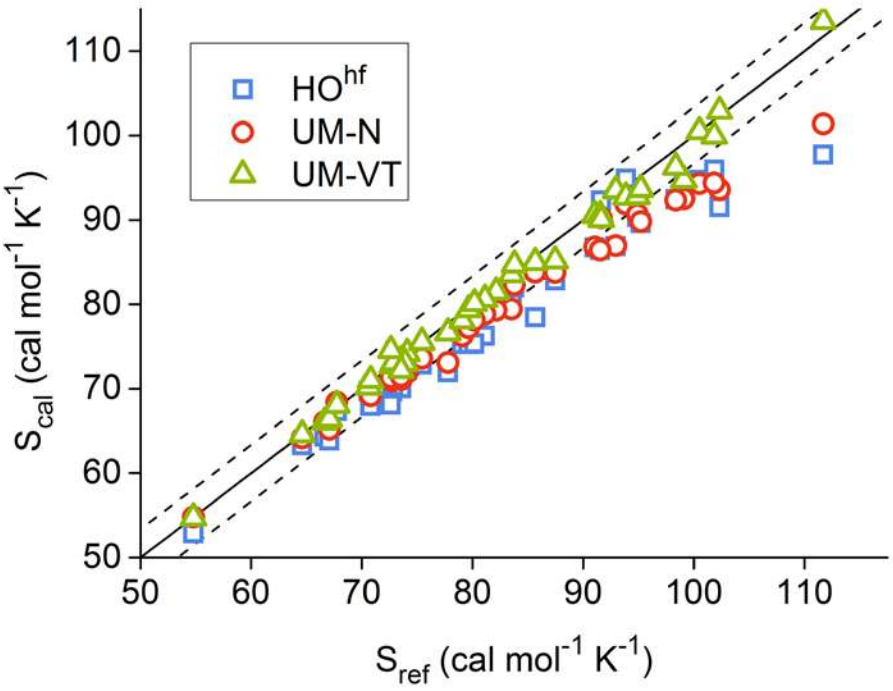

Figure 5. Parity plot of standard entropies listed in Table 2. An error bar of ± 3.35 cal mol^{-1} K^{-1} (equivalent to ± 1 kcal/mol of $\text{T} \cdot \text{S}$ at 298.15K) is shown by the dashed lines.

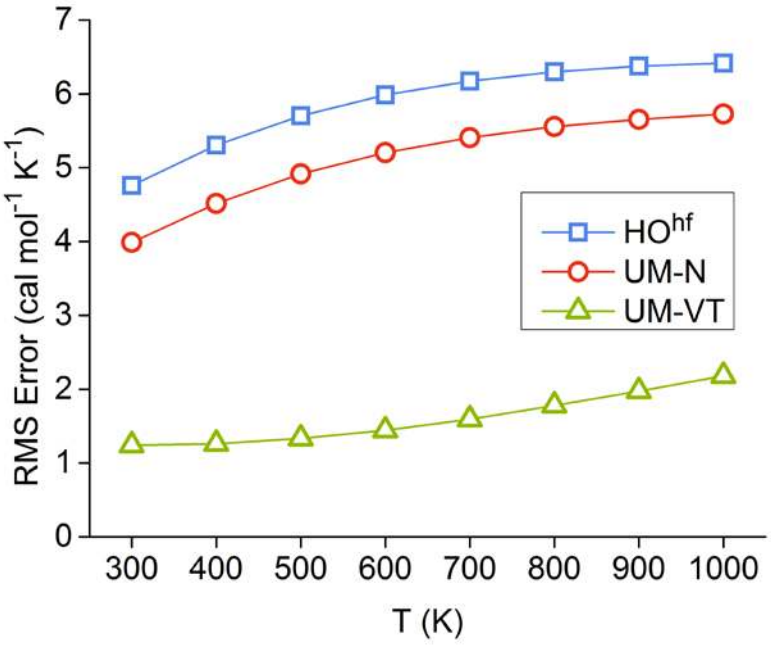

Figure 6. RMS errors of standard entropies of the species listed in Table 2.

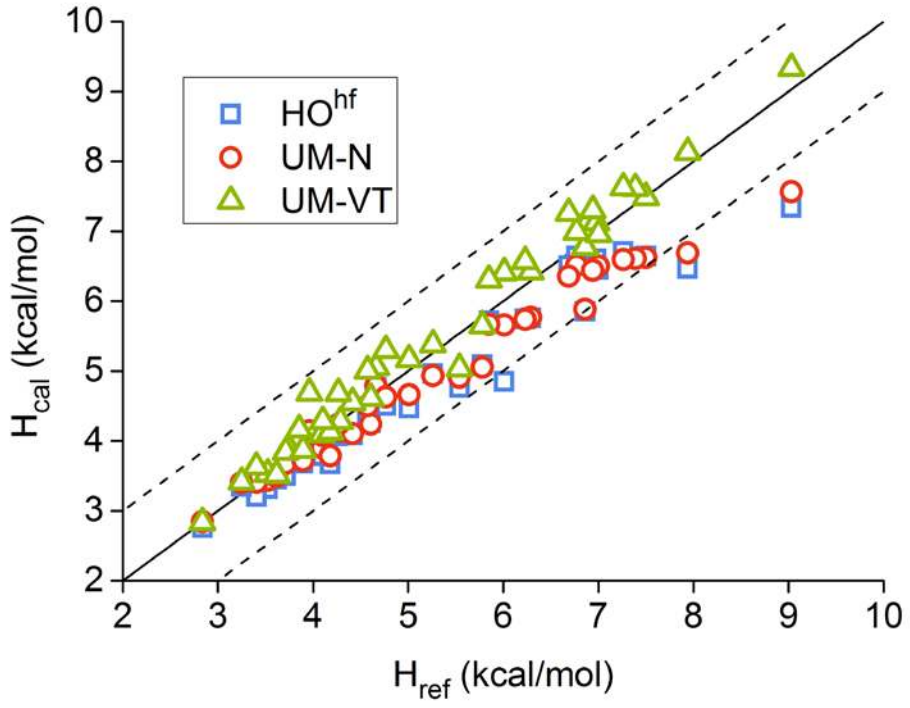

Figure 7. Parity plot of H(298.15K)-H(0K) listed in Table 3. An error bar of ± 1 kcal/mol is shown by the dashed lines.

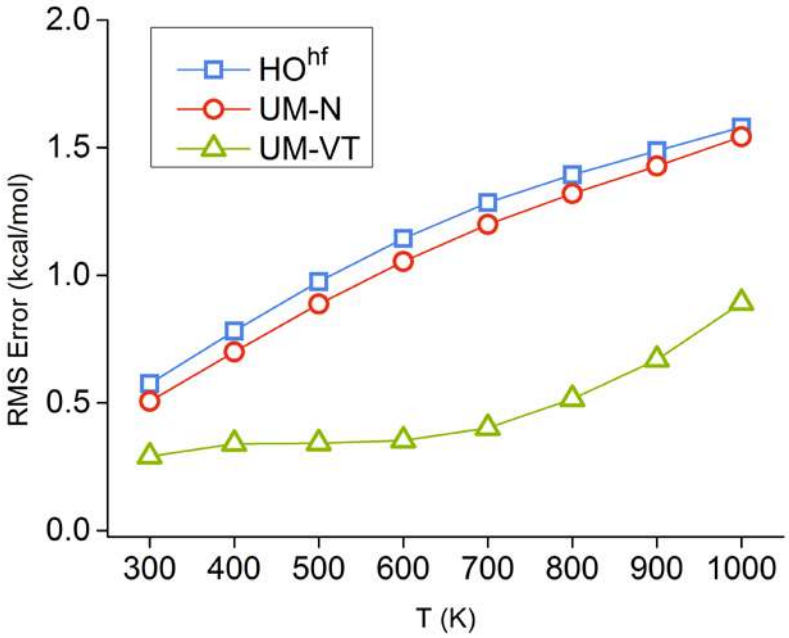

Figure 8. RMS errors of H(T)-H(0K) of the species listed in Table 3.

For Table of Contents Only